A computational view of the brain plasticity at rest

Invernizzi, Azzurra

DOI:
10.33612/diss.183130118

Chapter 4

Report on the application of Bayesian Connective Field modeling to primary open angle glaucoma

ABSTRACT

This report describes the preliminary results of the application of Bayesian Connective Field (CF) modeling to primary open angle glaucoma. In this study, we applied it to investigate whether glaucoma affects the functional organization of the visual cortex. We evaluated the CF size in glaucoma and healthy participants using both resting state (RS) and stimulus-driven fMRI data. As a second experiment, for each participant with glaucoma, a matched control participant observed the visual stimuli with a simulated scotoma (SS) that was designed to mimic the former's visual sensitivity as assessed using standard automated perimetry (SAP). By comparing results from these experiments and conditions, we can establish whether differences in CF size are a consequence of the ocular damage altering the visual input to the cortex. Our results show that in both RS and stimulus-driven conditions, the CF of the early visual areas are smaller in glaucoma compared to control participants. The smaller CF were not observed in the control group with SS. Neither was CF size correlated with the severity of glaucoma, as assessed using SAP and optical coherence tomography (OCT). We conclude that the observed changes in CF may be the result of neurodegeneration or local reorganization of the early visual cortex that appears to have developed at an early disease stage.

4.1 INTRODUCTION

Glaucoma is a neurodegenerative ophthalmic disease, which is characterized, amongst others, by ganglion cell loss and loss of visual field (VF) sensitivity. Recent brain imaging studies have shown that the degenerative damage is not limited to the eye and optic nerve but extends intracranially along the visual pathways and into the human visual cortex (Zhou et al. 2017; Lu et al. 2013). However, the extent to which this also affects the functioning of the adult visual cortex is not yet fully understood. The ability to establish this, as well as the presence of cortical adaptation (neuroplasticity) will be critical to assess the success of upcoming restorative therapies based on e.g. stem cells or cortical implants. However, establishing the presence of neuroplasticity is challenging in eye diseases such as glaucoma. Due to the disease, the visual input is already disrupted at the level of the eye. Such changes in input may result in spurious plasticity (Carvalho, Renken, and Cornelissen 2019; Binda et al. 2013; Haak, Cornelissen, and Morland 2012a; Heidi A. Baseler et al. 2011).

The issue of spurious plasticity may potentially be resolved by using resting-state (RS) fMRI recordings in combination with neural modelling of cortical functional connectivity. While a few studies have assessed local functional connectivity in glaucoma based on RS-fMRI data (Dai et al. 2013; Wang et al. 2016, 2017; Zhang et al. 2019), none of these studies have examined changes in the local spatial organization of these connections. A tool to specifically examine this is Connective Field (CF) modeling (see also chapters 2 and 3). It translates the concept of the stimulus-driven receptive field (RF) into the neural connectivity domain. The approach assesses the spatial dependency between signals in distinct cortical visual areas (Haak et al. 2013). The CF is also known as the cortico-cortical population receptive field. Assessing CF properties based on RS-fMRI potentially enables to assess cortical plasticity in the absence of stimulus-driven activity, thus removing this critical confound (Gravel et al. 2014; Invernizzi et al. 2021).

In this study, we applied Bayesian CF modeling to investigate how glaucoma affects the functional organization of the visual cortex. We evaluated the CF properties (position and/or size) of glaucoma and healthy participants using both RS and visual field mapping (VFM) fMRI data. By comparing results from these two conditions, we will be able to establish whether changes in CFs observed during RS are also present when stimuli are shown. As a second experiment, for each participant with glaucoma, a matched control participant observed the visual stimuli with a simulated scotoma (SS) designed to mimic the former's visual sensitivity as assessed using standard automated perimetry (SAP). Based on analysis of this data, we can establish whether any changes in CFs derived from stimulus-driven fMRI may be the result of altered visual input or

of cortical plasticity. Finally, the CF properties were correlated with the severity of glaucoma, as assessed by using SAP or optical coherence tomography (OCT).

4.2 METHODS

4.2.1 Study population

We recruited nineteen patients with primary open-angle glaucoma (POAG) and 22 healthy participants. One POAG participant dropped out of the study, therefore only 18 participants were included in this manuscript. Then, one age-matched control was assigned to each participant with glaucoma. This pairing was done based on the demographic parameters age and gender. The population demographics are shown in Table 1. Each participant participated in an ophthalmic session (for details, see next paragraph), followed by two MRI sessions. Prior to the ophthalmic assessment, participants signed an informed consent form. The ethics board of the University Medical Center Groningen (UMCG) approved the study protocol. The study followed the tenets of the Declaration of Helsinki.

Inclusion criteria for the participants with glaucoma were as follows: having an intraocular pressure (IOP) > 21 mmHg before treatment onset, presence of a VF defect (glaucoma hemifield test outside normal limits) due to glaucoma in at least one eye, abnormal OCT (peripapillary retinal nerve fiber layer thickness [pRNFL] at least one clock hour P<0.01), and spherical equivalent refraction within $\pm$3D. Exclusion criteria for both groups were: having any ophthalmic disorder affecting visual acuity (VA) or VF (other than POAG in the participants with glaucoma), any neurologic or psychiatric disorder, the presence of any abnormality or lesions in their magnetic resonance imaging (MRI) scans, or having any contraindication for MRI (e.g., having a pacemaker or being claustrophobic).

Table 1 - Demographics of participants with glaucoma and controls.

Measures	Participants with POAG (n = 18)		Healthy participants (n = 18)	
	Average	Standard Deviation	Average	Standard Deviation
Age	69.6	8.7	68.2	8.41
Gender (F%)	48%	-	34%	-
VA(R/L; decimal)	1/0.9	0.4/0.3	1.1/1	0.2/0.4
IOP(R/L; mmHg)	13.5/13.6	2.6/3.7	12.9/13.2	3.1/3.4
pRNFL thickness(R/L; μm)	70.2/65	11.6/9.6	97/97.6	7.9/7.5
VFMD (R/L; dB)	6.7/ 8.7	8.1/8.3	0.3/0.1	1.5/1.3

Average and standard deviation of age, percentage of female, intraocular pressure (IOP) for the right and left eye (average over three measurements), average peripapillary retinal nerve fiber layer (pRNFL) thickness and the VF mean deviation (VFMD) measured with HFA for the right and left eye. Note that all POAG participants were receiving treatment when recruited to this study.

4.2.2 Ophthalmic data

Prior to their participation in the MRI experiments, both glaucoma patients and controls underwent an ophthalmic screening, which included assessment of visual acuity (VA) , IOP, VF (Humphrey Visual Field Analyzer [HFA; Carl Zeiss Meditec, Jena, Germany] and structural assessment of the inner retina (Canon OCT-HS100; Canon, Tokyo, Japan). Results were expressed as the mean peripapillary retinal nerve fiber layer (pRNFL) thickness and the ganglion cell complex (GCC) thickness in the macular area. Visual acuity was measured using a Snellen chart with optimal correction provided for the viewing distance. IOP was measured using a Tonoref non-contact tonometer (Nidek, Hiroishi, Japan). For HFA we used the 24-2 grid with the Swedish Interactive Threshold Algorithm (SITA) Fast. Only reliable HFA tests were included in this study; a visual field test result was considered unreliable if false-positive errors exceeded 10% or if both fixation losses exceeded 20% and false-negative errors exceeded 10% (Wesselink and Jansonius 2017).

4.2.3 Visual stimulus presentation and description

The visual stimuli were displayed on an MR compatible display screen (BOLDscreen 24 LCD; Cambridge Research Systems, Cambridge, UK) located at the head-end of the MRI scanner with a viewing distance of 120 cm. The participant viewed the complete screen through a mirror placed at 11 cm from the eyes, supported by the 32-channel SENSE head coil. Screen size was 22 x 14 degrees of visual angle and the distance from the participant's eyes to the screen was approximately 120 cm. The maximum stimulus radius was 7 deg of visual angle. Stimuli were generated and displayed using the Psychtoolbox (https://github.com/Psychtoolbox-3/Psychtoolbox-3/) and VISTADISP toolbox (VISTA Lab, Stanford University), which ar both MatLab based (Brainard 1997; Pelli 1997).

4.2.3.1 Luminance contrast retinotopy stimulus

All participants underwent binocular visual field mapping (VFM) using a luminance contrast retinotopy (LCR) stimulus (Figure 1, panel A). The stimulus consisted of drifting bar apertures (of 10.2 deg radius) with a high contrast checkerboard texture on a grey (mean luminance) background. A sequence of eight different bar apertures with four different bar orientations (horizontal, vertical, and two diagonal orientations), two opposite motion directions, and four periods of mean-luminance presentations completed the stimulus presentation, which lasted 192 s. The bar contrast, width and spatial frequency were respectively 10%, 2.5 degrees and 0.5 cycles per degree. After each pass and a half, 12 seconds of a blank stimulus at mean luminance was presented full screen. To maintain stable fixation, participants were instructed to focus on a small colored dot present in the center of the screen and press a button as soon as the dot changed color. The complete visual field mapping paradigm was presented to the

participant four times, during four separate scans.

4.2.3.2 Luminance contrast retinotopy stimulus with a simulated scotoma superimposed

To control for the difference in visual perception between glaucoma and control participants, the control participants underwent an additional VF mapping where they viewed the LCR with a simulated scotoma (SS) superimposed. The SS for a control participant was designed to mimic the contrast sensitivity of the corresponding glaucoma participant under binocular vision. It was simulated by means of local reductions in contrast applied to the stimulus. For any control participant the SS consisted of an alpha transparency contrast layer that was based on the HFA sensitivity values of the participant with glaucoma with which they were matched. For example, a decrease of 3dB in HFA sensitivity is simulated by means of a reduction in stimulus contrast of 50%. The to be simulated decrease in HFA sensitivity was determined by averaging, for each test location, the left and right eye dB value in the total deviation plot of the glaucoma patient.

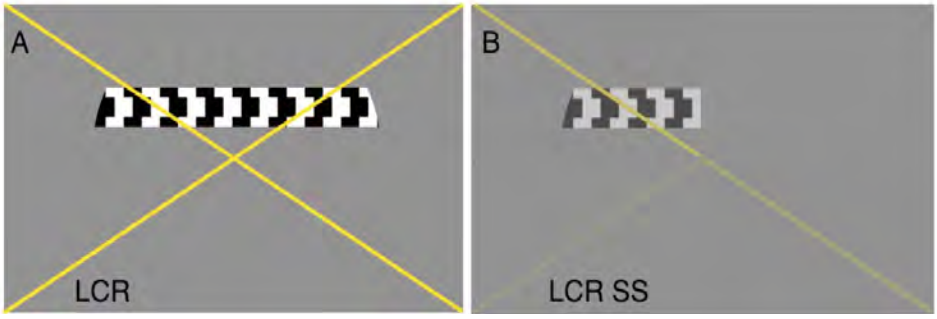

Figure 1 - Example of the stimuli used to obtain pRF parameter estimates. Panel A shows LCR stimulus and panel B reports an example of LCR SS stimulus. This particular example depicts the contrast sensitivity loss of participant G10 (MD (OD)=-8.37 dB; MD(OS)=-14.72 dB). The colour of the cross changed between yellow and black, and served to guide the gaze of the participant with central scotomas to the center of the cross.

4.2.4 Resting-state fMRI

During the RS-fMRI scans, the stimuli were replaced by a black screen and the lights in the scanning room were turned off. All participants were instructed to keep their eyes closed, lay as still as possible, to not fall asleep and to try to not think of anything in particular.

4.2.5 MRI and fMRI data acquisition procedure

Scanning was carried out on a 3 Tesla Siemens Prisma MRI-scanner using a 64-channel receiving head coil. In the first MRI session, an anatomical and two fMRI RS scans were acquired. A T1-weighted scan (voxel size, $1mm^3$; matrix size, 256 x 256 x 256) covering the whole-brain was recorded to chart each participant's cortical anatomy. Padding was used for a balance between comfort and reduction of head motion. The RS scans were collected using standard EPI sequence with duration of 260 seconds (TR, 1350 ms; TE, 30 ms; voxel size, $3mm^3$, flip angle 68; matrix size, 94 x 94 x 45). Slices were oriented to be approximately parallel to the calcarine sulcus.

In the second session, the retinotopic mapping took place. This session differed for participants with glaucoma and control participants. The control participants performed both the regular luminance contrast retinotopic mapping (LCR) and the LCR with a simulated scotoma (LCR SS) superimposed (Figure 1). The functional scans were collected using a standard EPI sequence (TR, 1500 ms; TE, 30 ms; voxel size, $3mm^3$, flip angle 80 ; matrix size, 84 x 84 x 24). Slices were oriented to be approximately parallel to the calcarine sulcus. For all retinotopic scans (LCR and LCR SS, see section 2.2.4), a single run consisted of 136 functional images (duration of 204 s). The (S) SPZ localizers consisted of 144 functional images (duration of 216 s). Prior to the first retinotopy scan, a short T1-weighted anatomical scan with the same field of view as chosen for the functional scans was acquired. This scan facilitated the co-registration between the functional and anatomical volumes.

4.2.6 Data analyses

Preprocessing and analysis of fMRI data were done using ITKGray (http://www.itk.org), Freesurfer (Fischl 2012), and mrVista toolbox for MatLab environment (VISTASOFT, http://vistalab.stanford.edu/; Engel, Glover, and Wandell 1997; Sereno, McDonald, and Allman 1994; Wandell and Winawer 2015). The Bayesian CF approach (for more details see Chapter 2) was developed and implemented in MatLab 2016b (The Mathworks Inc., Natick, Massachusetts).

For each participant, the structural, VFM, and RS functional MRI data were preprocessed. The structural scan was aligned in a common space defined using the anterior commissure-posterior commissure line (AC-PC line) as reference. Next, grey and white matter were automatically segmented using Freesurfer and manually adjusted using ITKGray (http://itk.org), in order to minimize segmentation errors. Then, all functional data were pre-processed using the mrVista toolbox. For both RS and VRM data the following steps are applied. First, head motion within and between scans were corrected by using robust multiresolution alignment of MRI brain volumes (Nestares and Heeger 2000), an alignment of functional data into anatomical space and an

interpolation of functional data with segmented anatomical grey and white matter. For RS-fMRI data, a few additional denoising steps were applied. These steps were possible as the RS scans were acquired for the whole brain. First, spatial smoothing at 6mm FWHM was applied in order to perform the denoising step based on ICA-AROMA that identified noise and motion related components (Pruim et al. 2015). These components were then removed from the unsmoothed and then, RS-fMRI data were filtered by applying a band-pass filter with a high-pass discrete cosine transform with cut-off frequency of 0.01 Hz and a low-pass 4th order Butterworth filter with a cut-off frequency of 0.1 Hz.

4.2.6.1 Population receptive field mapping

VFM scans were analyzed using a model-based analysis which allows localizing the visual field maps of interest, known as population receptive field (pRF) mapping (Dumoulin and Wandell 2008). In this analysis, for each voxel a pRF model (a 2D Gaussian) is convolved with the stimulus aperture and taking the hemodynamic response (HRF) into account, used to predict the BOLD response. Based on the best model fits, we estimate the visual field mapping parameters (eccentricity, polar angle and pRF size) per voxel. The parameters were projected onto a smoothed 3D mesh of the cortex. Using this analysis, the functional responses to the LCR VFM were analysed using a full field (FF) stimulus model. The data acquired in the LCR VFM SS condition in the control participants were analysed using this FF model and a model that included the SS. Based on the pRF model, the visual areas are outlined (V1, V2 and V3) to act as source (V1) or target region (V2, V3) for subsequent CF analyses.

4.2.6.2 Bayesian Connective Field mapping

CF models aim to explain the time-series for each location in the target region (V2 or V3) based on a linear combination of the time-series in the source region (V1; Haak et al. 2013b). The CF model is a 2D symmetric Gaussian kernel with the parameters CF position and CF size. For both VFM and RS data, we estimated the CF models using a Bayesian approach involving a Markov Chain Monte Carlo (MCMC) approach to efficiently sample the source region. The CF parameters associated with the best fitting model are converted from cortical units (cortical position) into visual field units (eccentricity and polar angle). This is done by inferring the pRF properties of the center voxel in the source region for each target location (Haak et al. 2013b). During a total of 17500 iterations, CF models were computed of which the results of the first 10% of iterations were discarded to allow burn-in (Chib 2011). The posterior probability distributions of the CF parameters were estimated based on the remaining samples. The estimated model values are projected on a smoothed 3D mesh.

4.2.7 Spatial analysis

For evaluating the pRF properties, only voxels were included with an explained variance (VE) > 30% and with an eccentricity > 1 deg and < 7 deg. For evaluating the CF properties, only voxels with an VE > 30% were included. These pRF and CF thresholds were chosen based on common practice in the current literature (H. A. Baseler et al. 2011; Haak, Cornelissen, and Morland 2012b; Winawer et al. 2010; Haak, Morland, and Cornelissen 2013). For each target voxel in V2 and V3, position information for their CF was based on the pRF of the center voxel of the weighted CF in the source region (V1). To investigate changes in CF properties between glaucoma and control participants, a cumulative distribution of each CF parameter was estimated at the participant level. Furthermore, the effect size (beta) was retained as an additional CF parameter as described in Chapter 2 (Invernizzi et al. 2020). Group level statistical testing was performed by first calculating the median across voxels per participant, and secondly, comparing these median values across groups (glaucoma vs control participants, glaucoma vs control participants with SS and finally, control participants vs control participants with SS). Based on a quantile analysis of the posterior distribution (Invernizzi et al., 2020), we computed a voxel-wise uncertainty measure for each CF parameter by subtracting the upper (Q_3) and lower (Q_1) quantile of the posterior distribution. The estimated uncertainty was computed for both RS and VFM data for each participant and repeated for each parameter directly estimated by the CF model (CF size and beta). Permutation analysis (10000 repetitions) with FWE correction applied for the number of group level comparisons was used. P-values <= 0.05 were considered significant. The correlation between CF size and disease severity was calculated using a linear fixed effects model, with a slope and intercept per participant as random effects. Finally, the intraclass correlation coefficient (ICC, (McGraw and Wong 1996; Perinetti 2018) was computed to estimate the test-retest reliability between the two RS-fMRI scans. As described in Chapter 3 (Invernizzi et al. 2021), the 5% most active voxels based on VE was used to compute the ICC score.

4.3 RESULTS

4.3.1 Cortical Topography

At the group level, no differences were found for any of the pRF parameters across the visual areas between the control participants (with and without SS) and the glaucoma participants (Figure S2).

Figure 2 shows that for the CF based on RS and VFM data, the topographical maps for eccentricity and polar angle were comparable and showed a clear visuotopic organization in both the healthy and glaucoma participants). Interestingly, only CF

size differs between glaucoma and healthy participants for both VFM and RS data (Figure 2). CF maps for RS2 scan are reported in supplementary material (Figure S1). Table 2 reports median and interquartile range at group level of each CF estimate. Interestingly, both glaucoma and age-matched healthy participants are characterized by small CF size.

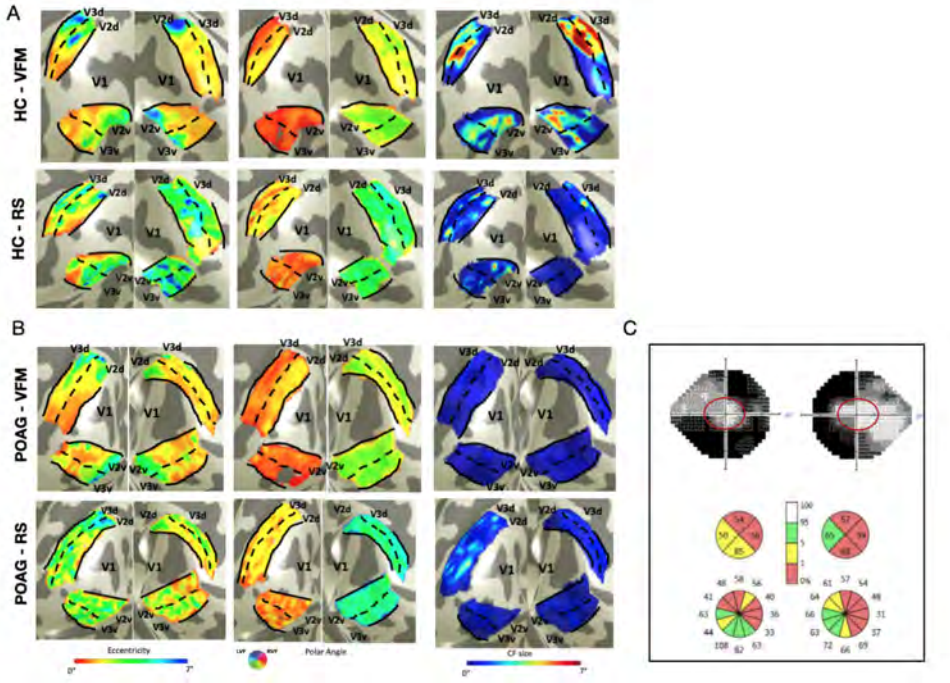

Figure 2. Topography of CF maps for VFM and RS-based fMRI for one control and one glaucoma participant. From left to right: eccentricity, polar angle and CF size obtained from VFM and RS data. Panels A and B show data for a glaucoma participant and an age matched control participant, respectively. It is notable that in the glaucoma participant a good retinotopic organization is maintained. Panel C shows the VF and OCT data for the glaucoma participant presented in panel B. Due to limited field of view (FOV) of stimulation (7deg), VFM data were collected only for the visual field area inside the red circle presented in panel C.

Table 2. Group median and interquartile range estimated based on VFM and RS data.

VFM

V1>V2	Control		Control SS		Glaucoma	
	median	IQR [Q1, Q3]	median	IQR [Q1, Q3]	median	IQR [Q1, Q3]
Eccentricity	3.633	[2.11, 6.85]	3.67	[1.81, 5.95]	2.26	[1.46, 4.82]
Polar Angle	2.55	[1.12, 3.96]	2.65	[1.08, 4.02]	2.48	[1.77, 3.73]
CF size	0.48	[0.15, 1.43]	0.52	[0.15, 1.08]	0.38	[0.15, 0.56]
Beta	1.18	[0.91, 1.49]	1.13	[0.89, 1.37]	1.35	[1.01, 1.68]
V1>V3	Control		Control SS		Glaucoma	
	median	IQR [Q1, Q3]	median	IQR [Q1, Q3]	median	IQR [Q1, Q3]
Eccentricity	4.19	[2.15, 6.62]	4.01	[1.963, 6.53]	2.49	[1.48, 4.34]
Polar Angle	2.56	[1.05, 4.03]	2.82	[1.08, 4.03]	2.9	[1.49, 3.78]
CF size	0.82	[0.21, 2.94]	0.67	[0.31, 1.48]	0.47	[0.17, 0.67]
Beta	1.21	[0.96, 1.47]	1.18	[0.93, 1.39]	1.45	[1.12, 1.78]

RS1

V1>V2	Control		Glaucoma	
	median	IQR [Q1, Q3]	median	IQR [Q1, Q3]
Eccentricity	3.82	[2.48, 6.89]	3.15	[1.90, 5.17]
Polar Angle	2.67	[1.42, 4.12]	2.29	[1.75, 3.57]
CF size	0.71	[0.21, 2.64]	0.5	[0.18, 0.76]
Beta	1.45	[0.99, 1.81]	1.46	[0.99, 1.87]
V1>V3	Control		Glaucoma	
	median	IQR [Q1, Q3]	median	IQR [Q1, Q3]
Eccentricity	4.02	[2.60, 6.56]	3.57	[1.93, 5.28]
Polar Angle	2.54	1.37, 3.95]	2.58	[1.38, 3.68]
CF size	0.62	[0.18, 2.04]	0.51	[0.18, 0.77]
Beta	1.29	0.95, 1.71]	1.41	[1.0, 1.81]

RS2

V1>V2	Control		Glaucoma	
	median	IQR [Q1, Q3]	median	IQR [Q1, Q3]
Eccentricity	3.81	[2.48, 6.89]	2.62	[1.63, 4.84]
Polar Angle	2.67	[1.42, 4.11]	2.25	[1.64, 3.58]
CF size	0.71	[0.21, 2.64]	0.48	[0.17, 0.69]
Beta	1.45	[0.99, 1.81]	1.7	[1.13, 2.20]
V1>V3	Control		Glaucoma	
	median	IQR [Q1, Q3]	median	IQR [Q1, Q3]
Eccentricity	4.02	[2.60, 6.56]	3.16	[1.88, 5.55]
Polar Angle	2.54	[1.37, 3.95]	2.37	[1.55, 3.47]
CF size	0.62	[0.18, 2.04]	0.43	[0.17, 0.65]
Beta	1.29	[0.95, 1.71]	1.69	[1.23, 2.12]

For eccentricity, polar angle, CF size, beta and the estimated uncertainty, the median and interquartile are computed at single subject level and then concatenated at group level for each ROIs separately.

Table 3. P-values obtained on the group median estimated based on VFM and RS data.

	p -values	Glaucoma vs Control		Glaucoma vs Control SS		Control vs Control SS	
		V1>V2	V1>V3	V1>V2	V1>V3	V1>V2	V1>V3
VFM	Eccentricity	**0.001**	**0.005**	**0.009**	**0.05**	0.76	0.32
	Polar Angle	0.55	0.41	0.96	0.8	0.65	0.22
	CF size	**0.003**	**0.002**	**0.001**	**0.001**	0.55	0.45
	Beta	0.12	**0.04**	**0.04**	**0.04**	0.66	0.68
	Unc. CF size	**0.04**	**0.005**	**0.02**	**0.001**	0.75	0.88
	Unc. Beta	0.52	0.65	0.37	0.44	0.92	0.99
RS1	Eccentricity	**0.01**	0.16				
	Polar Angle	0.43	0.73				
	CF size	**0.05**	0.06				
	Beta	0.57	0.53				
	Unc. CF size	**0.002**	**0.002**				
	Unc. Beta	0.13	0.18				
RS2	Eccentricity	**0.003**	0.12				
	Polar Angle	0.15	0.76				
	CF size	**0.004**	**0.03**				
	Beta	0.24	0.25				
	Unc. CF size	**0.001**	**0.01**				
	Unc. Beta	0.38	0.68				

Permutation analysis (10000 repetitions) with FWE correction applied for the number of group level comparisons was used. P-values <= 0.05 were considered significant.

4.3.2 Connective Field beta

Figure 3 shows the cumulative distributions of beta (effect size) for glaucoma and control participants as obtained during both VFM and RS-fMRI. Only for the VFM data, for both V1>V2 and V1>V3 significant differences between the glaucoma and control participants (with and without SS) were found (Table 3, panel VFM). No significant differences were found in either of the two RS scans (Table 3, panels RS1 and RS2). Moreover, Figure 4 shows the cumulative distribution of the uncertainty of beta for glaucoma and control participants. No significant differences were found between groups for either the VFM or RS data (Table 3).

4.3.3 Connective Field size

Figure 5 shows the cumulative distributions of CF size for glaucoma and control participants as obtained during both VFM and RS-fMRI. For VFM data, the CF size significantly differs between glaucoma and control participants (with and without SS) for both V1>V2 and V1>V3 (Table 3, VFM panel). The CF size differs in both RS scans only for V1>V2 (Table 3, RS1 and RS2 panels). The cumulative distributions for each subject of the second RS scan are shown in Figure S3. Figure 6 shows the cumulative distributions of the obtained uncertainty of CF size for glaucoma and control participants as obtained during both VFM and RS-fMRI. Similar to the CF size parameter, the uncertainty of CF size differs in both RS scans for V1>V2 but only in RS2 for V1>V3 (Table 3). Significant differences between glaucoma and control participants (with and without SS) were found for both V2 and V3 (Table 3). Note that in both CF size and related uncertainty, a floor effect is present in the glaucoma group. This is due to the minimum CF size (i.e.0.01) allowed by the MCMC model (Chapter 2, method).

4.3.4 Connective Field eccentricity

Figure 7 shows the cumulative distributions of CF eccentricity for glaucoma and control participants as obtained during both VFM and RS-fMRI. A significant difference between glaucoma and control participants was found for both VFM and RS data for V1>V2 but not V1>V3. The polar angle did not reach significance for any visual area or experimental condition (VFM- or RS-based, Figure S4).

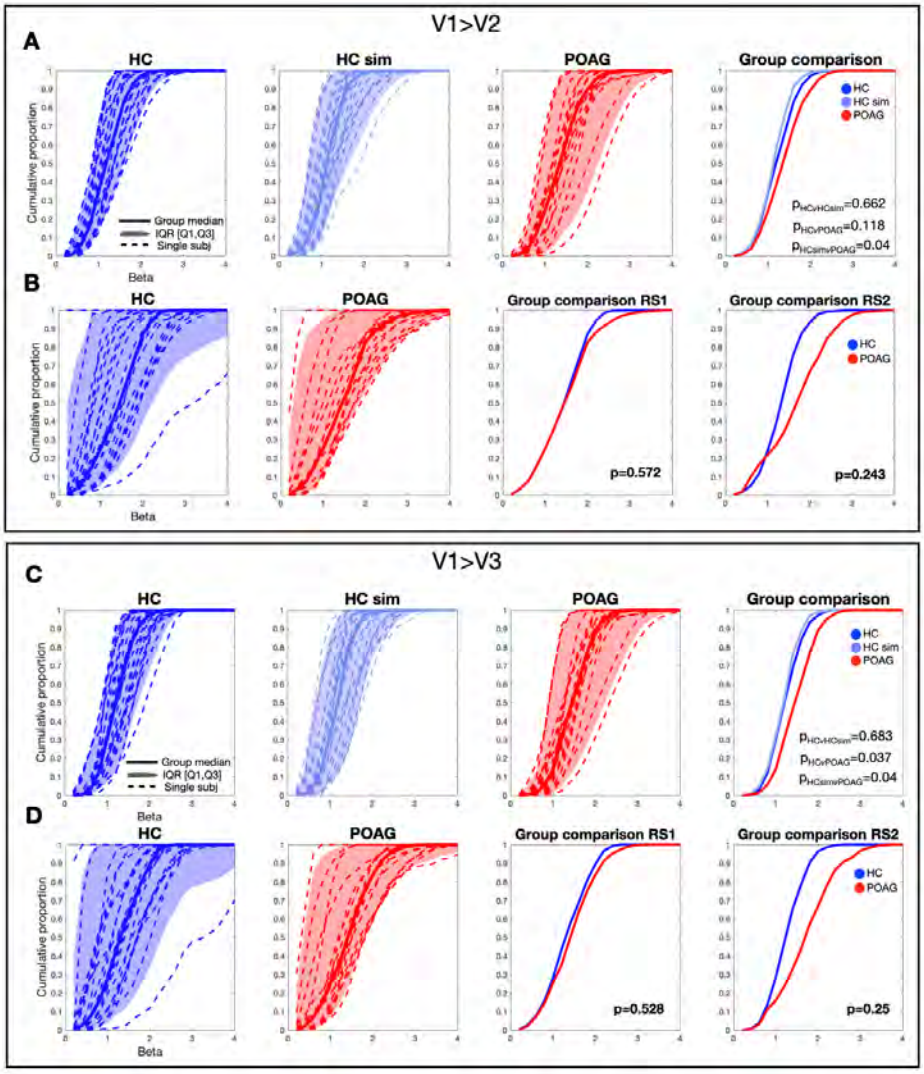

Figure 3. Cumulative distribution of beta at the group level based on VFM and resting-state data. The cumulative distribution of each single subject (dotted line), the group median (dash line) and the interquartile range are plotted for glaucoma (red), control (blue) and control with simulated scotoma (light blue). Panel A represents the cumulative proportion based on the VFM data for the three conditions. While panel B reported the cumulative proportion for each group based on the first RS scan and the median group comparison for both RS scans (RS1 and RS2).

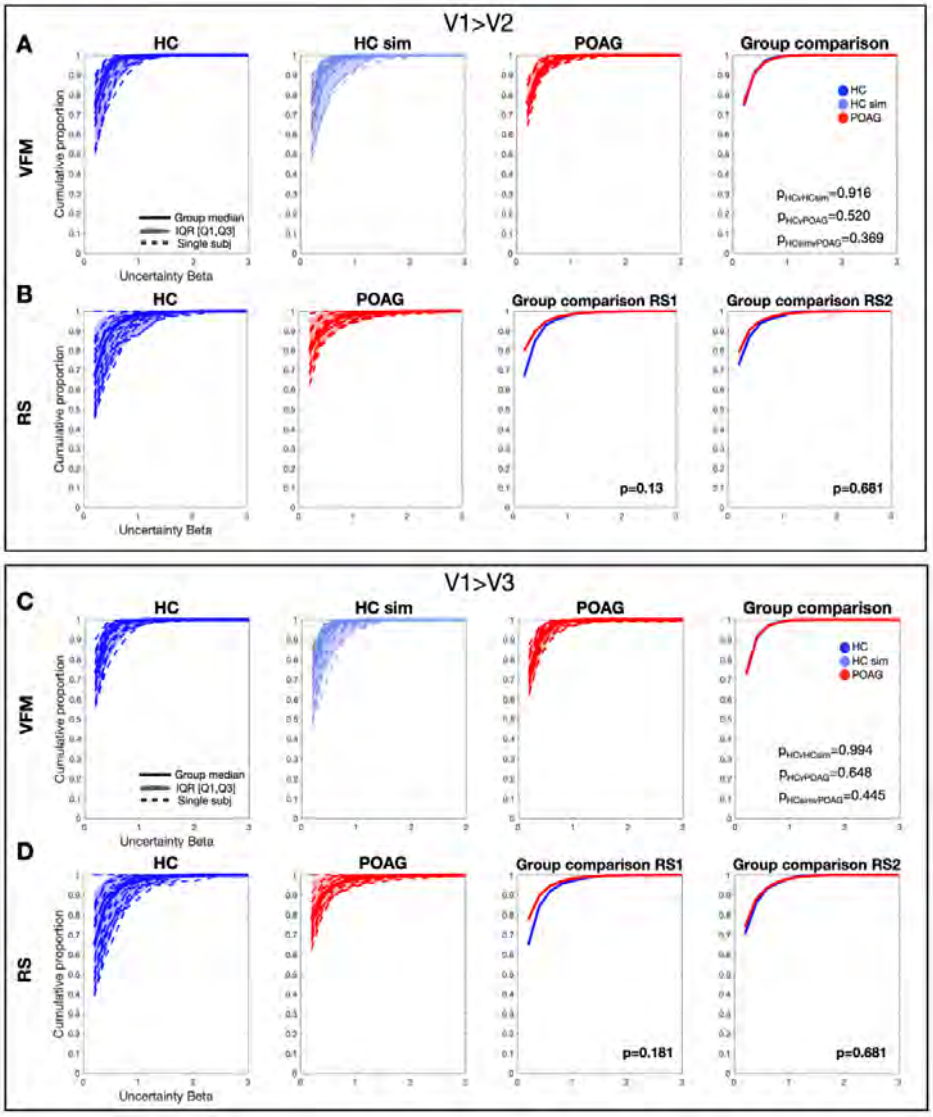

Figure 4. Cumulative distribution of the uncertainty of beta at the group level based on VFM and resting-state data. The cumulative distribution of each single subject (dotted line), the group median (dash line) and the interquartile range are plotted for glaucoma (red), control (blue) and control with simulated scotoma (light blue). Panel A represents the cumulative percentage based on the VFM data for the three conditions. While panel B reported the cumulative percentage for each group based on the first RS scan and the median group comparison for both RS scans (RS1 and RS2).

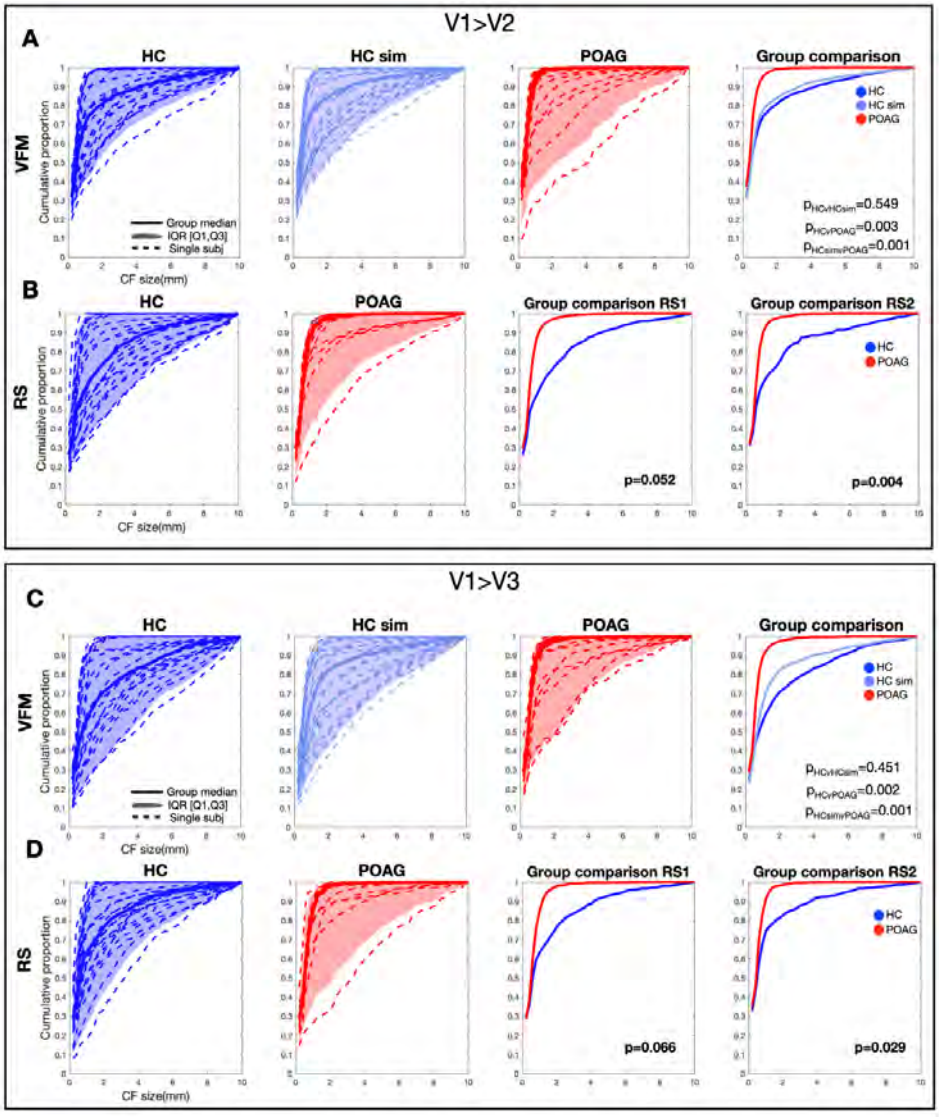

Figure 5. Cumulative distribution of connective field size at the group level based on VFM and RS fMRI data. The cumulative distribution of each single participant (dotted line), the group median (dash line) and the interquartile range are plotted for glaucoma (red), control (blue) and control with simulated scotoma (light blue). Panel A and C represent the cumulative percentage based on the VFM data for the three conditions. While panel B and D report the cumulative percentage for each group based on the first RS scan and the median group comparison for both RS scans (RS1 and RS2). The cumulative percentage for each single participant based on the second RS scan is reported in supplementary material.

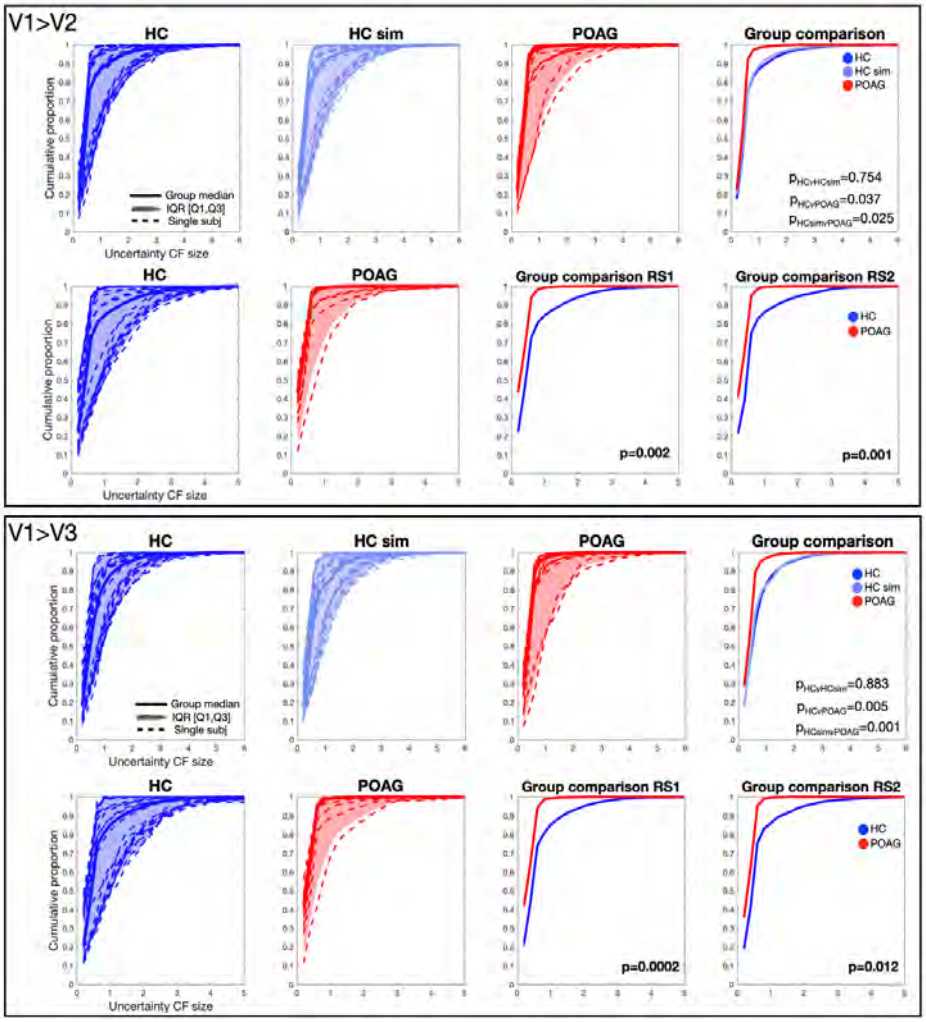

Figure 6. Cumulative distribution of uncertainty of connective field size at group level based on VFM and resting-state data. The cumulative distribution of each single subject (dotted line), the group median (dash line) and the interquartile range are plotted for glaucoma (red), control (blue) and control with simulated scotoma (light blue). Panel A represents the cumulative proportion based on the VFM data for the three conditions. While panel B reported the cumulative proportion for each group based on the first RS scan and the median group comparison for both RS scans (RS1 and RS2).

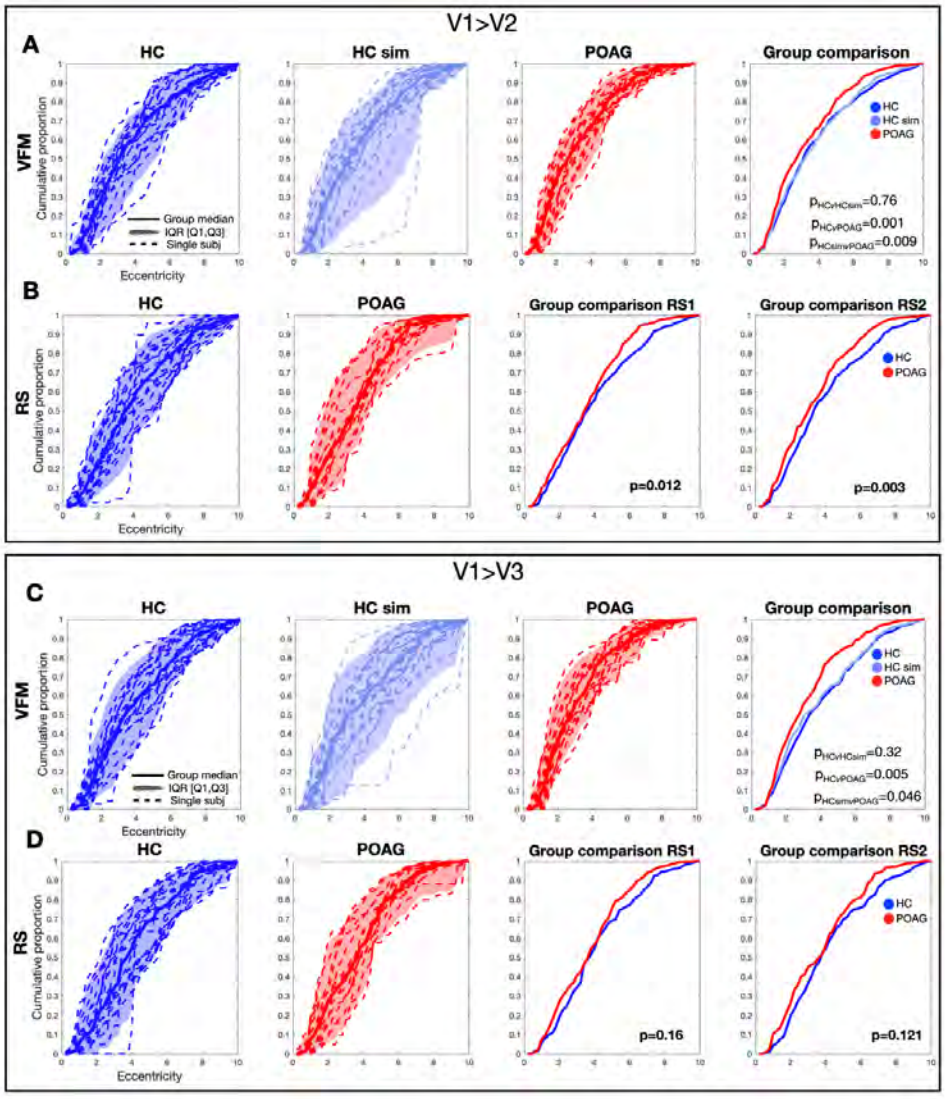

Figure 7. Cumulative distribution of CF eccentricity at the group level based on VFM- and RS fMRI data. The cumulative distribution of each single participant (dotted line), the group median (dash line) and the interquartile range are plotted for glaucoma (red), control (blue) and control with simulated scotoma (light blue). Panel A and C represent the cumulative percentage based on the VFM data for the three conditions. While panel B and D report the cumulative percentage for each group based on the first RS scan and the median group comparison for both RS scans (RS1 and RS2). The cumulative percentage for each single participant based on the second RS scan is reported in supplementary material.

4.3.5 CF size as a function of glaucoma severity

Figure 8 shows a correlation between the average VFM-based CF size of the individual visual field (VF) quadrants (within 7 degrees) and the GCC thickness in the corresponding quadrant. For both control and glaucoma participants for CF of V1>V2, a non-significant negative correlation was found. For V1>V3 CFs, the correlation plots are reported in the supplementary materials (Figure S6). Furthermore, we report the correlations based on RS2 data (Figure S7).

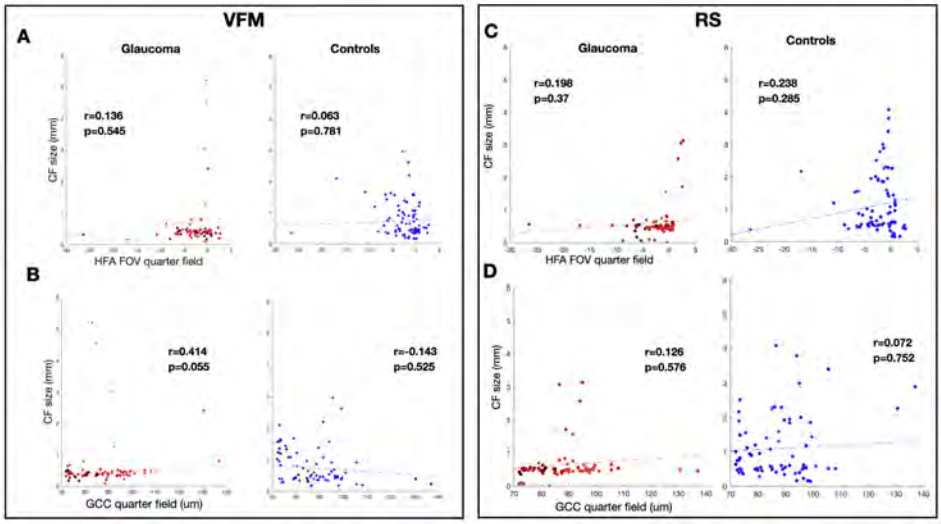

Figure 8. CF size for V1>V2 as a function of either HFA or OCT data of glaucomatous participants. Correlation of CF size VFM-based obtained from individual quadrants with HFA and GCC from healthy and glaucoma participants. HFA values were calculated as mean deviation of both eyes combined. GCC thickness was calculated by averaging the thickness of the macula of both eyes. Each data point is from a separate quadrant of an individual participant. Panels B and D show the correlations of VFM- and RS-based CF size with GCC value, respectively.

4.4 DISCUSSION

We observed differences between glaucoma and control participants in the functional spatial integration that occurs between visual brain areas. Specifically, based on brain activity recorded during both visual stimulation and resting-state conditions, we found shifts in the position and reductions in the size of the CFs . Of relevance, no differences were observed in the estimates of effect size (beta) or in its associated uncertainty. This indicates that the differences were not due to a low signal quality or caused by a poor fit of the CF models to the data in either of the groups. Moreover, our results are consistent over two resting-state scans (supplementary material, test-retest).

At the same time, we observed that the coarse retinotopic organization of the early visual cortex in glaucoma patients is preserved, which is in line with previous findings in other pathology (Papanikolaou et al. 2014; H. A. Baseler et al. 2011). Thus, while the retinotopic organization of the visual areas is maintained, the way in which the primary visual cortex propagates the visual information to higher order visual areas (and v.v.) differs between glaucoma and age-matched healthy controls. In other words, the way in which early visual areas communicate with one another differs between groups. We find these differences in both the presence and absence of visual stimulation (Figure 5 and 7). Simulating scotoma in age-matched controls does not result in similar differences.

Furthermore, there is no correlation between CF size and glaucoma severity (either in terms of VF sensitivity or thickness of the ganglion cell complex (Figure 6). Together, this indicates that the differences are not directly related to the amount or quality of the signals that are passed on from the eyes to the brain. Moreover, due to the limited field of view (FOV) of stimulation in the scanner (7deg) we primarily evaluated the cortical projection zone of the central visual field. Together with the fact that glaucomatous visual field defects start out in the visual periphery, this implies that the differences in cortical visual information processing are not a mere consequence of glaucoma affecting the eye. Moreover, it thus seems that these differences may already be present at an early stage of glaucoma.

4.4.1 Limitations and future studies

Due to the limited field of view (FOV) of stimulation we could not evaluate peripheral visual cortical regions that are affected by advanced stages of glaucoma. Moreover, the majority of the scotomas that we could study were due to relatively small reductions in contrast sensitivity. By studying participants with more advanced glaucoma and scotomas with binocular overlap within the MRI FOV it could be investigated whether the observed differences in CF properties would be more profound in such cases.

Another limitation is the heterogeneity of the participants with glaucoma for which we were not able to control. This resulted in differences in the extent of their scotoma, in asymmetries of the visual field defects in both eyes, and differences in disease duration and progression which may all have affected the differences in CF. To better understand the origin of the CF differences, future studies may include more homogenous groups as the mentioned factors might affect the degrees of neurodegeneration or functional reorganization. Finally, the latter factors may potentially affect the delineation of the visual areas. For this reason, future studies could consider the use of anatomy-based or probabilistic maps to define the visual brain areas (Wang et al. 2015).

The MR acquisition protocols between VFM and RS scans were slightly different in our present study. However, the CF estimates obtained with RS and VFM scans agreed well. Nevertheless, as mentioned in chapter 3 as well, future studies should consider using identical MR parameters for the VFM and RS scans.

4.5 CONCLUSION

Glaucoma affects the spatial properties of the functional connections between the primary and later visual cortical areas. Moreover, the resulting change in functional integration shows neither a relation to disease stage nor can be directly attributed to a reduced stimulation of the visual cortex due to the ocular defect. This suggests these changes may either be a result of neurodegeneration or functional reorganisation in the early visual cortex that already occured at an early stage of the disease.

REFERENCES

Baseler, H. A., A. Gouws, K. V. Haak, C. Racey, Crossland, A. Tufail, G. S. Rubin, F. W. Cornelissen, and A. B. Morland. 2011. "Large-Scale Remapping of Visual Cortex Is Absent in Adult Humans with Macular Degeneration." *Nature Neuroscience* 14 (5). https://doi.org/10.1038/nn.2793.

Baseler, Heidi A., André Gouws, Koen V. Haak, Christopher Racey, Michael D. Crossland, Adnan Tufail, Gary S. Rubin, Frans W. Cornelissen, and Antony B. Morland. 2011. "Large-Scale Remapping of Visual Cortex Is Absent in Adult Humans with Macular Degeneration." *Nature Neuroscience* 14 (5): 649–55.

Binda, Paola, Jessica M. Thomas, Geoffrey M. Boynton, and Ione Fine. 2013. "Minimizing Biases in Estimating the Reorganization of Human Visual Areas with BOLD Retinotopic Mapping." *Journal of Vision* 13 (7): 13.

Brainard, David H. 1997. "The Psychophysics Toolbox." *Spatial Vision*. https://doi.org/10.1163/156856897x00357.

Carvalho, J., R. J. Renken, and F. W. Cornelissen. 2019. "Studying Cortical Plasticity in Ophthalmic and Neurological Disorders: From Stimulus-Driven to Cortical Circuitry Modeling Approaches." *Neural Plasticity* 2019 (November). https://doi.org/10.1155/2019/2724101.

Chib, Siddhartha. 2011. "Introduction to Simulation and MCMC Methods." In *The Oxford Handbook of Bayesian Econometrics*. Oxford University Press.

Dumoulin, S. O., and B. A. Wandell. 2008. "Population Receptive Field Estimates in Human Visual Cortex." *NeuroImage* 39 (2). https://doi.org/10.1016/j.neuroimage.2007.09.034.

Engel, S. A., G. H. Glover, and B. A. Wandell. 1997. "Retinotopic Organization in Human Visual Cortex and the Spatial Precision of Functional M RI." *Cerebral Cortex* 7 (2). https://doi.org/10.1093/cercor/7.2.181.

Gravel, Nicolás, Ben Harvey, Barbara Nordhjem, Koen V. Haak, Serge O. Dumoulin, Remco Renken, Branislava Curčić-Blake, and Frans W. Cornelissen. 2014. "Cortical Connective Field Estimates from Resting State fMRI Activity." *Frontiers in Neuroscience* 8 (October): 339.

Haak, Koen V., Frans W. Cornelissen, and Antony B. Morland. 2012a. "Population Receptive Field Dynamics in Human Visual Cortex." *PloS One* 7 (5): e37686.

———. 2012b. "Population Receptive Field Dynamics in Human Visual Cortex." *PloS One* 7 (5): e37686.

Haak, Koen V., Antony B. Morland, and Frans W. Cornelissen. 2013. "Connective Field Estimates in the Cortical Lesion Project Zone of Individuals with Macular Degeneration." *Journal of Vision* 13 (15): T11–T11.

Haak, Koen V., Jonathan Winawer, Ben M. Harvey, Remco Renken, Serge O. Dumoulin, Brian A. Wandell, and Frans W. Cornelissen. 2013. "Connective Field Modeling." *NeuroImage* 66 (February): 376–84.

Invernizzi, Azzurra, Nicolas Gravel, Koen V. Haak, Remco J. Renken, and Frans W. Cornelissen. 2021. "Assessing Uncertainty and Reliability of Connective Field Estimations From Resting State fMRI Activity at 3T." *Frontiers in Neuroscience* 15 (February): 625309.

Invernizzi, Azzurra, Koen V. Haak, Joana C. Carvalho, Remco J. Renken, and Frans W. Cornelissen. 2020. "Bayesian Connective Field Modeling: A Markov Chain Monte Carlo Approach." *Cold Spring Harbor Laboratory*. https://doi.org/10.1101/2020.09.03.281162.

Lu, P., L. Shi, H. Du, B. Xie, C. Li, S. Li, T. Liu, H. Feng, and J. Wang. 2013. "Reduced White Matter

Integrity in Primary Open-Angle Glaucoma: A DTI Study Using Tract-Based Spatial Statistics." *Journal of Neuroradiology = Journal de Neuroradiologie* 40 (2). https://doi.org/10.1016/j.neurad.2012.04.001.

McGraw, Kenneth O., and S. P. Wong. 1996. "Forming Inferences about Some Intraclass Correlation Coefficients." *Psychological Methods*. https://doi.org/10.1037/1082-989x.1.1.30.

Papanikolaou, A., G. A. Keliris, T. D. Papageorgiou, Y. Shao, E. Krapp, E. Papageorgiou, K. Stingl, et al. 2014. "Population Receptive Field Analysis of the Primary Visual Cortex Complements Perimetry in Patients with Homonymous Visual Field Defects." *Proceedings of the National Academy of Sciences of the United States of America* 111 (16). https://doi.org/10.1073/pnas.1317074111

Pelli, Denis G. 1997. "The VideoToolbox Software for Visual Psychophysics: Transforming Numbers into Movies." *Spatial Vision*. https://doi.org/10.1163/156856897x00366

Perinetti, Giuseppe. 2018. "StaTips Part IV: Selection, Interpretation and Reporting of the Intraclass Correlation Coefficient." *South European Journal of Orthodontics and Dentofacial Research*. https://doi.org/10.5937/sejodr5-17434.

Sereno, Martin I., Colin T. McDonald, and John M. Allman. 1994. "Analysis of Retinotopic Maps in Extrastriate Cortex." *Cerebral Cortex* 4 (6): 601–20.

Wandell, B. A., and J. Winawer. 2015. "Computational Neuroimaging and Population Receptive Fields." *Trends in Cognitive Sciences* 19 (6). https://doi.org/10.1016/j.tics.2015.03.009

Wang, Liang, Ryan E. B. Mruczek, Michael J. Arcaro, and Sabine Kastner. 2015. "Probabilistic Maps of Visual Topography in Human Cortex."

Cerebral Cortex 25 (10): 3911.

Wesselink, Christiaan, and Nomdo M. Jansonius. 2017. "Glaucoma Progression Detection with Frequency Doubling Technology (FDT) Compared to Standard Automated Perimetry (SAP) in the Groningen Longitudinal Glaucoma Study." *Ophthalmic & Physiological Optics: The Journal of the British College of Ophthalmic Opticians* 37 (5): 594–601.

Winawer, J., H. Horiguchi, R. A. Sayres, K. Amano, and B. A. Wandell. 2010. "Mapping hV4 and Ventral Occipital Cortex: The Venous Eclipse." *Journal of Vision* 10 (5). https://doi.org/10.1167/10.5.1.

Zhou, Wei, Eric R. Muir, Kundandeep S. Nagi, Steven Chalfin, Pavel Rodriguez, and Timothy Q. Duong. 2017. "Retinotopic fMRI Reveals Visual Dysfunction and Functional Reorganization in the Visual Cortex of Mild to Moderate Glaucoma Patients." *Journal of Glaucoma* 26 (5): 430–37.

SUPPLEMENTARY MATERIAL

Test-Retest

To estimate test-retest reliability between the two RS scans, we selected the 5% most active voxels and computed the ICC scores for each CF parameter obtained from RS1 and RS2 scans. The arbitrary threshold level for CF estimates was chosen based on (Invernizzi et al. 2021). A positive ICC value is reported for all CF parameters and across all rois (Figure S5, V1>V2 - panel A; V1>V3 - panel B).

SUPPLEMENTARY FIGURES

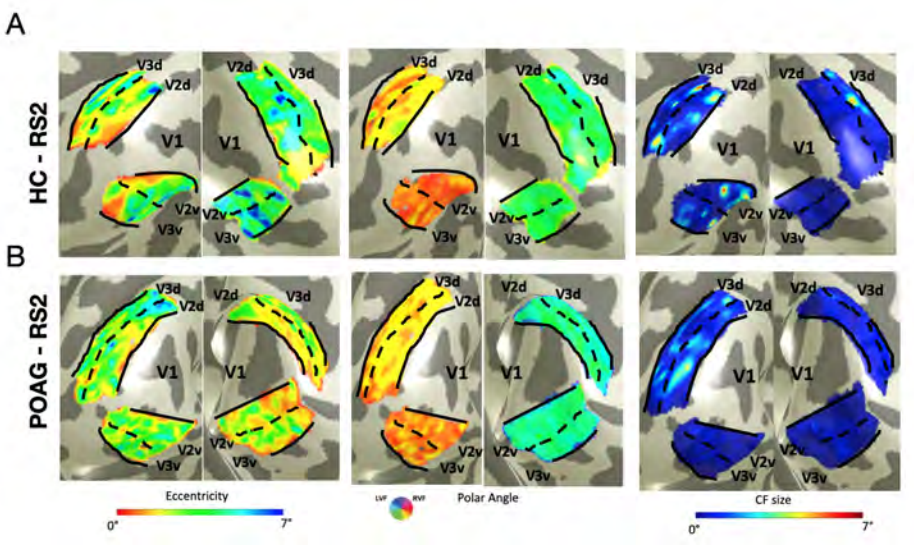

Figure S1. Visualization of CF maps based on RS2 scan for one control and one glaucoma participant. From left to right: eccentricity, polar angle and CF size parameters obtained from RS2 data. Panel A corresponds to an age-matched healthy participant, while Panel B to a glaucoma participant.

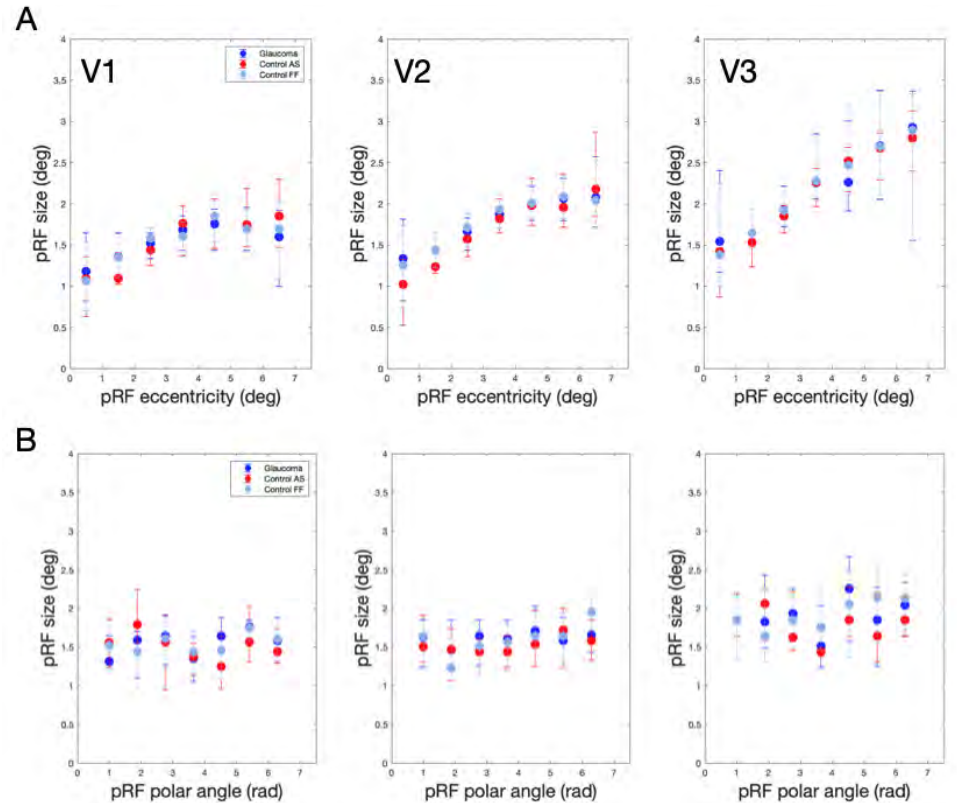

Figure S2. pRF properties at group level. Average pRF eccentricity (panel A) and polar angle (panel B) are plotted in function of the pRF size for each early visual area analysed (V1, V2 and V3). Eccentricity was binned in bins of 1 deg. Average results were obtained by pairing each glaucoma (red dot) with control with (light blue dot) and without simulated scotoma (blue dot). Error bars indicate the standard error of the mean over hemisphere.

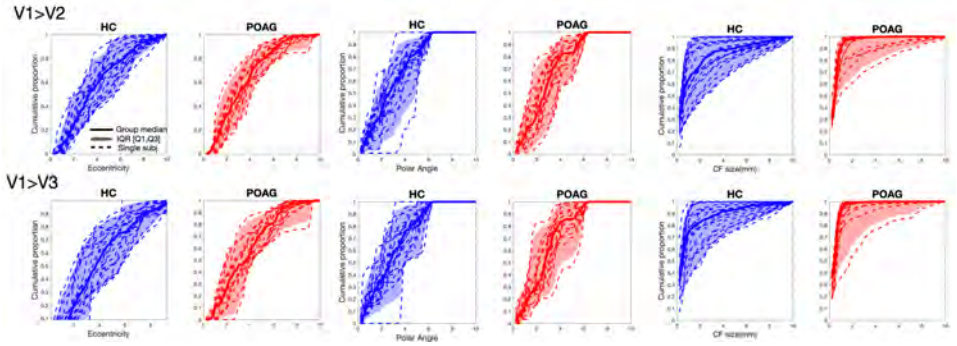

Figure S3. Cumulative distribution of each CF parameter based on second resting-state data. The cumulative distribution of each single subject (dotted line), the group median (dash line) and the interquartile range are plotted for glaucoma (red) and control (blue). From left to right: eccentricity, polar angle and CF size parameters obtained from RS2 data.

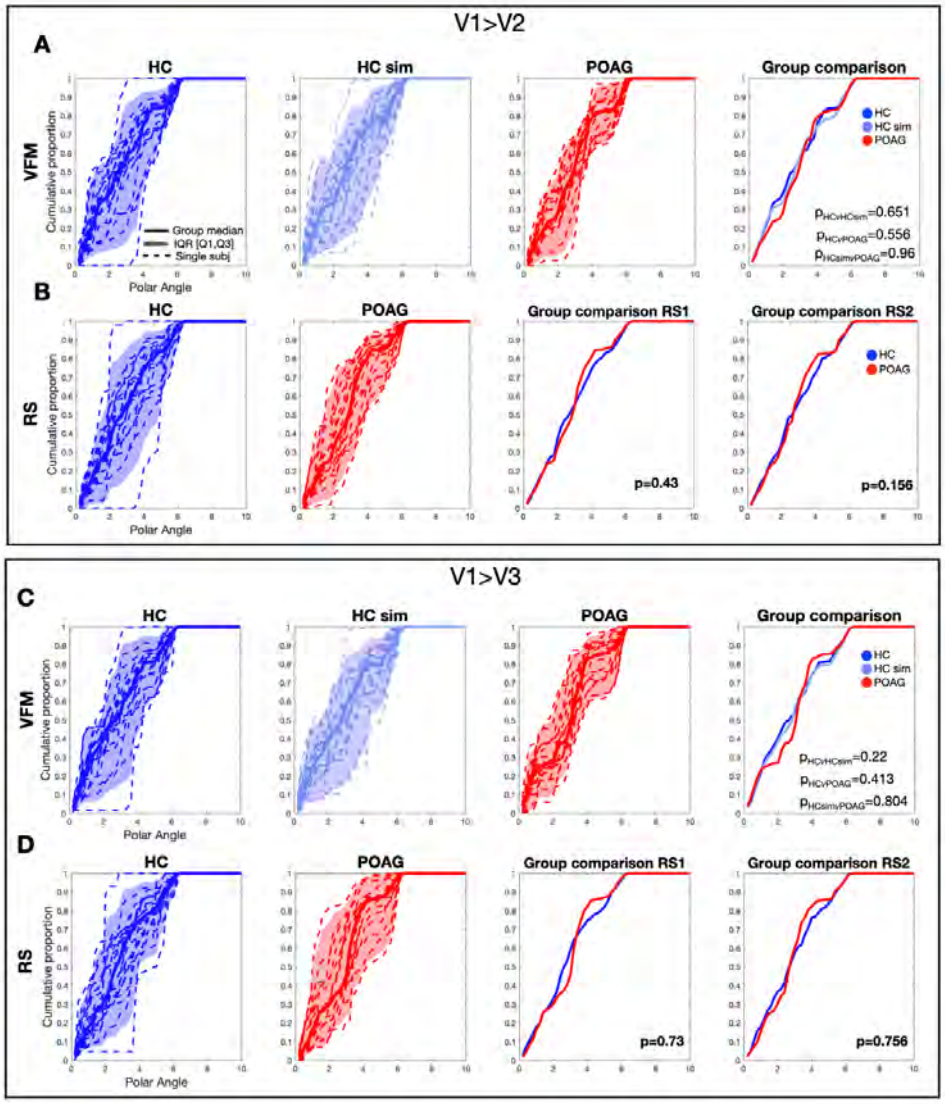

Figure S4. Cumulative distribution of polar angle at group level based on VFM and resting-state data. The cumulative distribution of each single subject (dotted line), the group median (dash line) and the interquartile range are plotted for glaucoma (red), control (blue) and control with simulated scotoma (light blue). Panel A represents the cumulative percentage based on the VFM data for the three conditions. While panel B reported the cumulative percentage for each group based on the first RS scan and the median group comparison for both RS scans (RS1 and RS2).

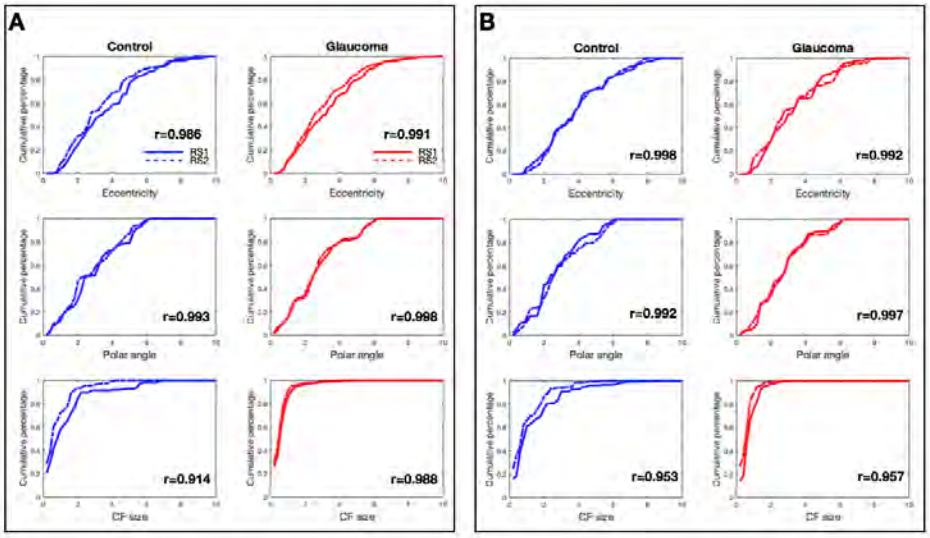

Figure S5. Test-retest evaluation between RS scans. The median group cumulative distributions of each CF parameter are plotted for RS1 (line) and RS2 (dashed line). Panel A represents the cumulative percentage for V1>V2 and panel B reports the ones for V1>V3. Intraclass correlation coefficients (ICC) were calculated across all paired participants and for each roi separately.

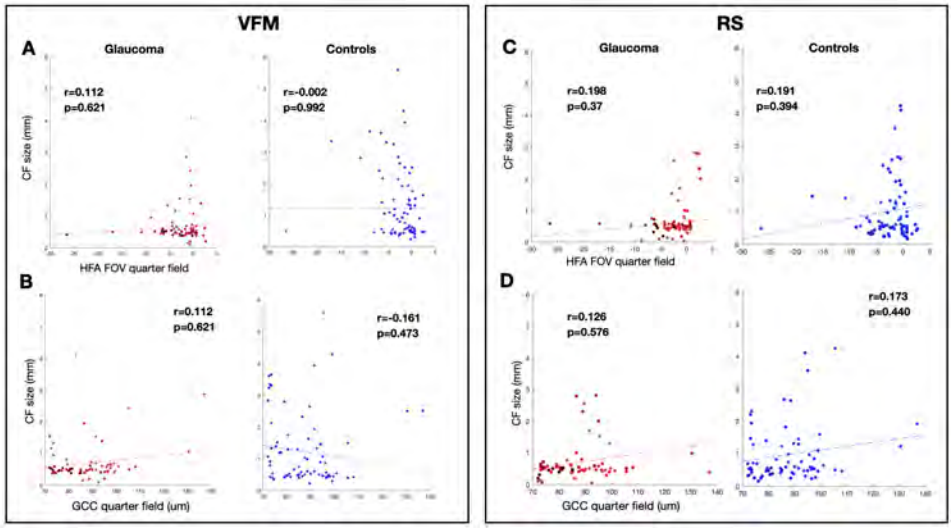

Figure S6. CF size as a function of glaucoma severity based on HFA and OCT data of V1>V3 area. Correlation of CF size VFM- and RS1-based obtained from individual quadrants with HFA and GCC from healthy and glaucoma participants. HFA values (MD) as calculated by averaging the thickness of the macula of both eyes. While, GCC thickness was calculated by averaging the thickness of the macula of both eyes. Each data point is from a separate quadrant of an individual participant with glaucoma. Panels A and C report the correlation plot of CF size VFM- and RS-based with HFA, respectively. Panels B and D report the correlation plot of CF size VFM- and RS-based with GCC value, respectively.

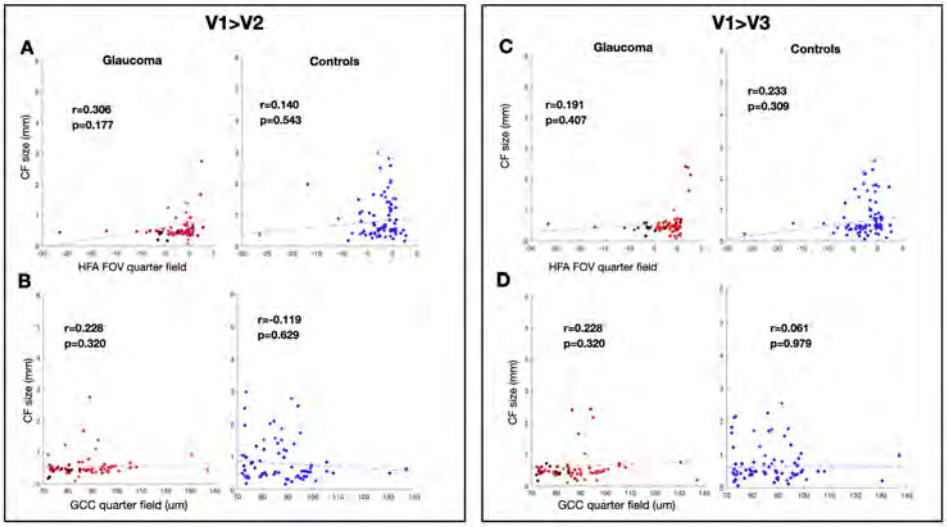

Figure S7. CF size RS2-based as a function of glaucoma severity based on HFA and OCT data of V1>V3 area. Correlation of CF size RS2-based obtained from individual quadrants with HFA and GCC from healthy and glaucoma participants. HFA values (MD) as calculated by averaging the thickness of the macula of both eyes. While, GCC thickness was calculated by averaging the thickness of the macula of both eyes. Each data point is from a separate quadrant of an individual participant with glaucoma. Panels A and C report the correlation plot for HFA. Panels B and D report the correlation plot for GCC values.